


# ADAMS model validation for an all-terrain vehicle using test track data

Advances in Mechanical Engineering  
2019, Vol. 11(7) 1–18  
© The Author(s) 2019  
DOI: 10.1177/1687814019859784  
journals.sagepub.com/home/ade  


Husain Kanchwala<sup>1</sup>  and Anindya Chatterjee<sup>2</sup>

## Abstract

MD ADAMS® is widely used for vehicle suspension modeling. In this article, we present modeling, simulation, and test track evaluation of an all-terrain recreational vehicle. Our intention is to study the degree to which simplified ADAMS modeling actually matches human-driven vehicle response. For suspension model validation, a vehicle is generally tested on a four-poster test rig and base excitation is applied at four ground-wheel contacts. However, actual driving experience does not match idealized testing conditions. In this work the vehicle is manually driven on a variety of tracks at different speeds, and the vertical accelerations at four axle locations and four body points are measured. The same are then compared in detail against predictions from ADAMS simulation with vertical base excitation. The contribution of this article is in identifying those aspects of the simulation results that match experiments well and identifying possible sources for the observed mismatch, especially under more severe test conditions.

## Keywords

All-terrain vehicle, ADAMS model, suspension, model validation, field testing

Date received: 14 March 2019; accepted: 4 June 2019

Handling Editor: James Baldwin

## Introduction

ADAMS is widely used for accurate vehicle dynamics simulation.<sup>1–3</sup> A practical problem commonly addressed in the vehicle dynamics literature is that of validating and refining the ADAMS model so as to match experimental results better. For such model refinement and validation, four-poster test rigs are commonly used for commercial applications<sup>4–6</sup> (see also Banerjee et al.<sup>7</sup>). However, actual driving experience may differ from that suggested by idealized testing conditions. A related question, more relevant for small all-terrain vehicles (ATVs) on uneven ground, is as follows: to what extent is the ADAMS model able to predict what is actually experienced by the vehicle in the hands of a human driver?

For this latter question, comparisons between model predictions and actual test track data are more suitable.<sup>8</sup> This article presents a useful contribution in that direction.

In this article, ADAMS model development and subsequent field testing of an ATV is presented. The vehicle used is a single-seater prototype of mass approximately 150 kg, built for an all-terrain racing competition<sup>9</sup> by undergraduate engineering students.<sup>10</sup>

It will be seen below that the match obtained varies with ride conditions and demands (this is not surprising; see, for example, Els<sup>11</sup>). On relatively gentle tracks, the human rider is better able to maintain a constant speed, the vehicle frame flexes less as well, and overall a better match is obtained. On more severe tracks,

<sup>1</sup>Centre for Electronic Warfare, Information and Cyber, Cranfield University, Defence Academy of the United Kingdom, Shrivenham, UK  
<sup>2</sup>Mechanical Engineering, Indian Institute of Technology Kanpur, Kanpur, India

### Corresponding author:

Husain Kanchwala, Defence Academy of the United Kingdom, Shrivenham SN6 8LA, UK.  
Email: h.kanchwala@cranfield.ac.uk



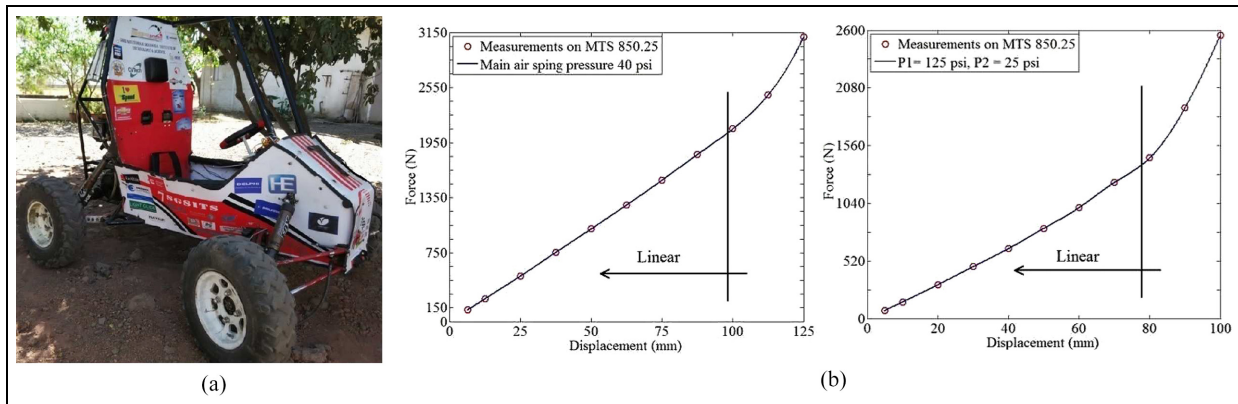


**Figure 1.** (a) ATV used for field testing and (b) force versus displacement characteristics of front suspensions (main pressure = 40 psi) and rear suspensions (EVOL pressure, P1 = 125 psi; main pressure, P2 = 25 psi).

especially with twisting loads on the chassis, we find that rider movement, chassis flexibility, and speed variations are all more significant, and a poorer match is obtained.

There are two main activities involved in this work: model development and field testing.

In the modeling part, suspension components were tested and an ADAMS model was developed. A wheel-ground kinematic model was used to calculate inputs for the ADAMS model. Finally, the vehicle response was simulated. In the testing part, the vehicle was instrumented and then driven at several constant speeds on several tracks. Measured accelerometer outputs were compared against the model predictions.

In what follows, ADAMS model development is described in section “Vehicle model development in ADAMS.” The road-wheel contact model is discussed in section “Road contact kinematic model.” The testing procedures are described in section “Vehicle testing.” Model simulation and field test results are presented in section “Results.” The effect of frame flexibility and a potential application of our modeling approach for simulating other standard test tracks is also discussed in section “Results.” Final comments and future scope of this work are given in section “Discussion and conclusion.”

We hope that this study will lead to a better understanding of what a human driver may actually encounter, especially in a small vehicle on rough ground, and the extent to which such conditions can be incorporated into straightforward ADAMS models.

## Vehicle model development in ADAMS

### Vehicle suspension

The ATV used for field testing is shown in Figure 1(a).

The vehicle has a double wishbone front suspension and a semi-trailing arm rear suspension. The front and rear suspensions are equipped with FOX Float 3 and Float 3 EVOL (“extra volume”) R pneumatic shock absorbers, respectively. The suspension characteristics were measured on an MTS 850.25 damper test rig at NATRiP, Indore.<sup>12</sup>

Force versus displacement characteristics of front and rear suspensions are shown in Figure 1(b). For the given air pressure setting and in the useful range of suspension travel, these characteristics are seen to be linear. The suspension damping properties were not measured in this study, but obtained from damper charts.<sup>13</sup>

Suspension component properties used in the ADAMS model for both front and rear suspensions are reported in Table 1.

Because of the suspension linkage kinematics, the shock absorber compression differs from the wheel travel. In the ADAMS model below, the suspension spring and dampers will be treated as purely vertical. Such a simplification is routinely made in many industrial studies to avoid the complications of the linkages. To use this trick, suspension component stiffness and damping values must be multiplied by a motion ratio (squared). These motion ratios were experimentally obtained by raising/lowering the wheel of interest and measuring the spring compression/extension and were found out to be 0.64 and 0.66 for front and rear suspensions, respectively.

Using these suspension properties, a simplified ADAMS model was built (see also Kanchwala and Chatterjee<sup>14</sup> for some additional details).

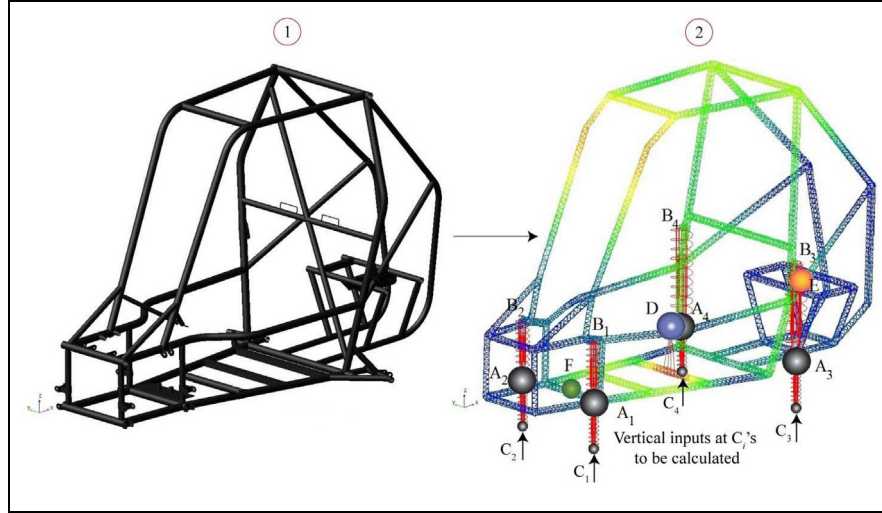
### ADAMS model

The vehicle chassis is made of a roll cage-type structure. The physical and material properties of the roll cage

**Table 1.** Typical values of suspension properties obtained from suspension characterization and equivalent properties at wheels.

Identifier	$K_{\text{front}}$ (N/mm)	$K_{\text{rear}}$ (N/mm)	$C_{\text{front}}$ (N s/mm)	$C_{\text{rear}}$ (N s/mm)
Suspension	25	15	1.50	1.36
At wheels	10.5	6.5	0.63	0.59

The equivalent suspension properties at wheels are obtained after multiplying by the square of the motion ratios.

**Figure 2.** ① CAD model of the chassis. ② FE model of the simplified chassis with pipe curvatures removed. The displacement inputs are given to wheel contact points  $C_i$ .**Table 2.** Structural details, vehicle mass, and inertial properties.

Identifier	Value
Material and cross section	Steel AISI 4130 (circular)
Diameter and thickness	31.75 and 1.65 mm
Yield and ultimate strength	721 and 760 MPa
CG location ( $X$ , $Y$ , and $Z$ )	812, 0, and 580 mm
Sprung mass ( $M_s$ )	165 kg
Inertias ( $I_x$ , $I_y$ , $I_z$ and $I_{yz}$ )	257, 246, 24, and 41 kg m <sup>2</sup>

members, center of gravity location (from front axle above the ground), vehicle mass, and inertia properties are given in Table 2. The material properties were measured by the ASTM A370-2012 tensile test.<sup>15</sup> From the computer-aided design (CAD) model of the chassis (see ① in Figure 2), a simplified geometrical model was built and a finite element (FE) model of the latter was developed in Nastran as shown in ②. The FE model was then imported into ADAMS. The four mounting locations  $B_i$  were defined as interface nodes. In addition, the model had three more interface nodes denoted as D, E, and F, corresponding to the center of mass locations of the driver, engine, and battery, respectively (see

**Table 3.** Unsprung mass and tire properties.

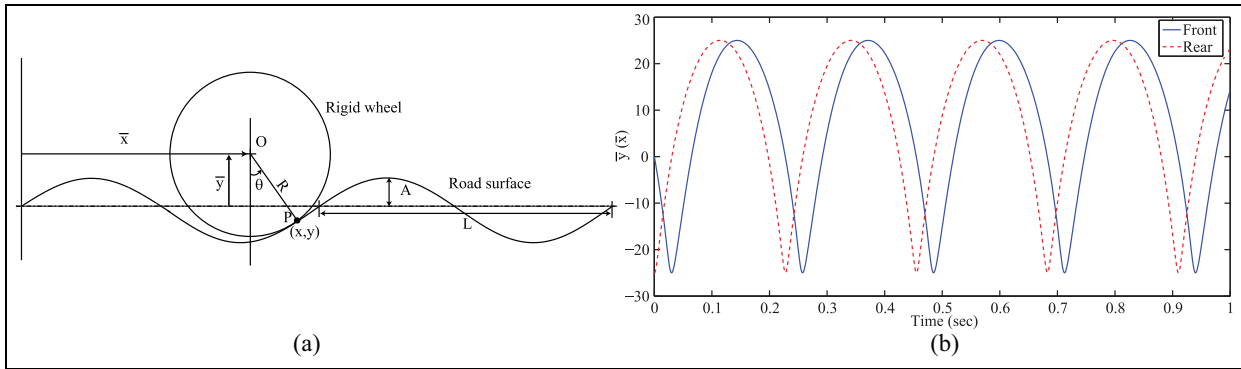
Identifier	Front	Rear
$M_u$ (unsprung mass)	15 kg	12.5 kg
$K_t$ (tire stiffness)	40 N/mm	40 N/mm
$C_t$ (tire damping)	0.2 N s/mm	0.2 N s/mm

② in Figure 2). Three rigid bodies with mass and inertia properties representing the driver, engine-driveline assembly, and battery were attached to these interface nodes. (These interface nodes are in turn connected to the FE mesh using RBE2 elements, which connects rigid body nodes to a few nodes in the deformable mesh.) The inertia properties of driver were obtained from previous studies<sup>16,17</sup> and that of engine and batteries were obtained from the CAD assembly.<sup>10</sup>

Four spring-dashpot pairs with the equivalent properties from Table 1 are attached between points  $B_i$  on the car body and unsprung masses at wheel axle  $A_i$ . The unsprung masses are further connected by springs and dashpots representing tire properties to ground contact points  $C_i$ . The unsprung mass and tire properties are listed in Table 3. The vehicle is equipped with 22x7-10

**Table 4.** Continuous displacement track and test details.

S. no.	Track	Severity	Amplitude (mm)	Pitch (mm)	Test speed (kmph)
1	Washboard	Low	15	400	7.5
		High	25	600	11
2	Herringbone	Low	10	500	9
		High	20	800	19
3	Chassis twist	Low	150	2000	7.5
		High	200	4000	14.5
4	One-sided washboard	High	25	600	13

**Figure 3.** (a) Kinematics of a rigid wheel going over a sinusoidal road and (b) the road displacement input acting on the wheel contact point P as seen at O. This particular road displacement input is for the vehicle running at a speed of 9.5 kmph on high-severity washboard track.

BKT W207 ATV tires<sup>18</sup> in all four wheels, but the front wheel has greater mass because of a brake assembly. Note that ATV tires use low inflation pressures (typically 7 psi) and have low stiffness and high damping compared to typical commercial tires.

### Road contact kinematic model

The half-wavelength of the sinusoidal tracks is comparable to the tire diameter, and although the road profile is sinusoidal, the actual *displacement input* to the wheel is not sinusoidal. The road surface geometry has to be converted into an equivalent vertical input to be applied at the wheel-ground contact points  $C_i$  of the simplified ADAMS model. We use a simple road contact kinematic model that calculates the effective wheel displacements for the continuous displacement tracks (see Table 4).

Consider a rigid wheel going over a sinusoidal track as shown in Figure 3(a). The track amplitude is  $A$ , wavelength is  $L$ , and tire radius is  $R$ . The coordinates of wheel center  $O$  is  $(\bar{x}, \bar{y})$  and the coordinates of the wheel-ground contact point  $P$  is  $(x, y)$ . From geometrical considerations

$$x = \bar{x} + R \sin \theta \quad (1)$$

$$y = A \sin \left( \frac{2\pi x}{L} \right) \quad (2)$$

$$\frac{dy}{dx} = \tan \theta \quad (3)$$

Differentiating equation (1) gives

$$\dot{x} = \dot{\bar{x}} + R \dot{\theta} \cos \theta \quad (4)$$

where  $\dot{\bar{x}}$  is the vehicle longitudinal velocity, taken as a constant ( $v$ ). Substituting equation (2) in equation (3) and differentiating the same gives

$$\dot{\theta} = -A \left( \frac{2\pi}{L} \right)^2 \sin \left( \frac{2\pi x}{L} \right) \dot{x} \cos^2 \theta \quad (5)$$

Using equations (4) and (5) yields

$$\dot{x} = \frac{v}{1 + AR \cos^3 \theta \left( \frac{2\pi}{L} \right)^2 \sin \left( \frac{2\pi x}{L} \right)} \quad (6)$$

$$\dot{\theta} = \frac{-Av \left( \frac{2\pi}{L} \right)^2 \sin \left( \frac{2\pi x}{L} \right) \cos^2 \theta}{1 + R \cos^3 \theta A \left( \frac{2\pi}{L} \right)^2 \sin \left( \frac{2\pi x}{L} \right)} \quad (7)$$



**Figure 4.** Test tracks used, left to right: washboard, herringbone, chassis-twist, one-sided washboard, and Belgian pave.

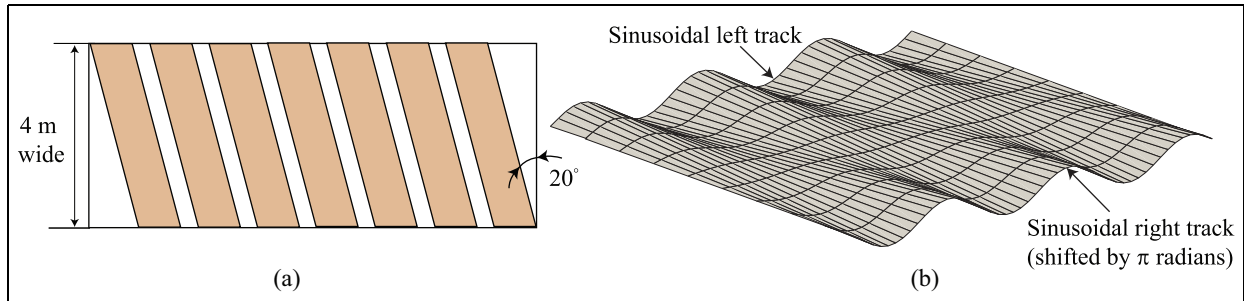


**Figure 5.** Schematic layouts of (a) herringbone and (b) twist tracks, respectively.

Equations (6) and (7) are solved numerically in MATLAB using `ode45` with initial conditions  $x = \bar{x} = (L/4)$ ,  $\theta = 0$  at  $t = 0$ . A typical solution is shown in Figure 3(b). These computed ground excitations are used as cubic spline inputs for all deterministic ADAMS simulations in this article.

In the above approach for calculating displacement inputs, the deformation of the wheel is neglected but the shifting of the contact location is accounted for using rigid wheel kinematics.

During ADAMS simulation, the consequent vertical displacement input is directly applied at points  $C_i$  (see  $\textcircled{2}$  in Figure 2). Therefore, in addition to the displacement input computed above, wheel stiffness and damping need to be assigned in the ADAMS model before final simulation. These quantities were estimated from the tire inflation pressure based on data for similar tires in Wong.<sup>19</sup> The stiffness and damping values used for model development are 40 N/mm and 0.2 N s/mm, respectively. Note that the tire compliance is a lot smaller than the suspension compliance, so small errors in the compliance estimates have tiny effects.

## Vehicle testing

The vehicle was instrumented with capacitor-based ADXL326 accelerometers (a total of eight) before performing field testing. The data acquisition system

consists of a FAT32 Micro SD card module and an Arduino ATmega328P micro-controller board. These systems are breadboard compatible, making it easy to connect them together and power the circuit by a 9 V battery.

Next, the vehicle was tested on various specialized test tracks at NATRiP, Indore<sup>20</sup> (see Figure 4). These test tracks are broadly classified into two types, namely continuous and discontinuous, as discussed below.

### Continuous displacement input tracks

These tracks have a simple displacement profile suited for deterministic simulation. Four tracks were selected under this category.

1. *Washboard track.* This is the simplest sinusoidal track. Inputs to the left and right wheels are identical.
2. *Herringbone track.* In this track, the bumps are inclined at an angle of 20 degrees across the width of the track (Figure 5(a)). The road inputs for the left and right wheels are no longer identical; the phase difference between them depends on the vehicle width.
3. *Chassis twist track.* This is a 4-m-wide track. The left and right track ends are sinusoids separated in phase by  $\pi$  radians (see Figure 5(b)). Between the two extreme profiles on right and left, the variation is linear (ruled patch).<sup>21</sup>



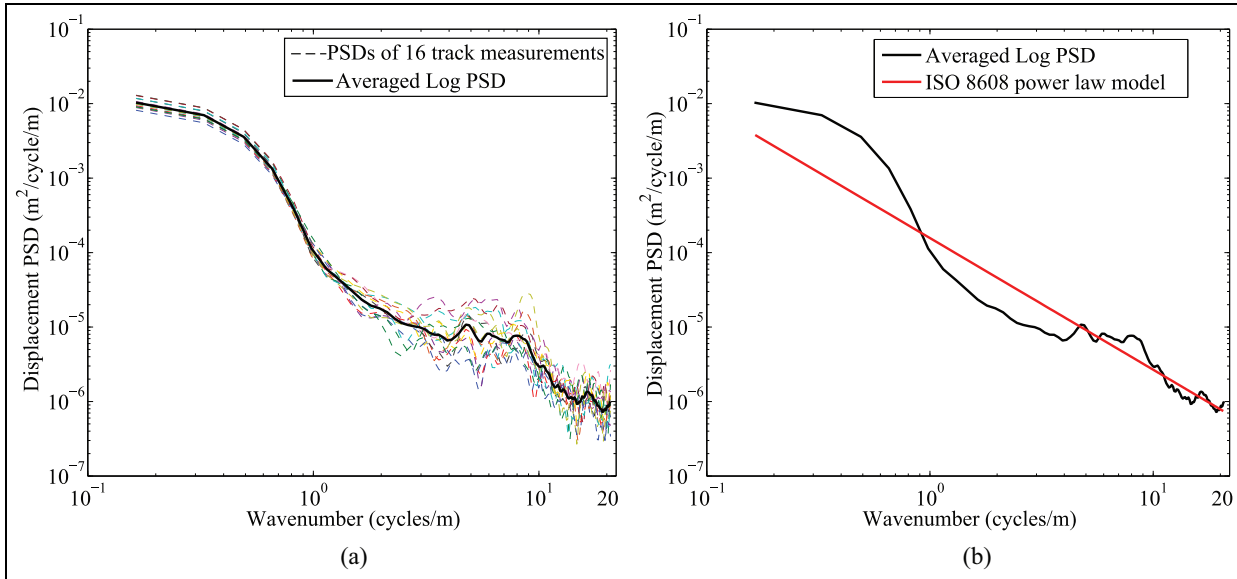


**Figure 6.** (a) Displacement PSDs obtained from the track measurement data and (b) ISO 8608 road model fitted on the averaged logarithm of the displacement PSD.

During testing, because our vehicle was relatively narrow, it was driven on one side of the track to increase the intensity of excitation at one wheel, at the cost of reducing the intensity at the other wheel (see Figure 4).

4. *One-sided washboard track.* This is identical to a washboard track, but here the ground excitation acts only on the left wheels.

Track and test details reported in this article are presented in Table 4 (some further tests and results are reported in Kanchwala<sup>22</sup> but not reproduced here for the sake of brevity).

#### *Discontinuous displacement input track: Belgian pave*

The tracks used so far for field testing have deterministic road inputs. We now consider the method of modeling terrain with generic road profiles using power spectral densities (PSDs) of the ground elevation.

The Belgian pave track is often used to simulate random terrains.<sup>23</sup> Its surface is made up of immovable cobbles (see Figure 4).

For this track, a stochastic model is used to describe the displacement inputs. The track width is 4 m. Elevations at different locations are measured at intervals of 150 mm in the longitudinal direction, and 250 mm in the lateral direction, giving 16 sets of

longitudinal profile measurements covering the track width. These measurements were made using the Can-Can Profilometer and the elevation data was provided by NATRiP.

Such road profiles are characterized by their PSD.<sup>24</sup> From the 16 sets of longitudinal profile measurement data, displacement PSDs were obtained using the `pwelch` function in MATLAB (see Figure 6(a)). For modeling, the ISO 8608 road model was used wherein a power law model was fitted to the logarithmic average displacement PSDs.<sup>25</sup> The fitted model was

$$S_Z(\Omega) = C \left( \frac{\Omega}{\Omega_0} \right)^{-w}, \quad C = 2.4e - 4, \quad w = 1.754 \quad (8)$$

where  $\Omega$  is the spatial angular frequency,  $\Omega_0 = 1$  rad/m, and the degree of unevenness  $C$  and waviness  $w$  are fitted parameters. The model fit is shown in Figure 6(b). The relatively large mismatch in the upper left part is actually for four low-frequency points which were left out of the fit; the rest of the match is reasonable. ADAMS computes a frequency domain response based on inputs as per equation (8). Road elevation PSDs are widely used in the literature for modeling different kinds of non-deterministic (random) terrains (see Figure 7).

Belgian pave tracks are also widely used for vehicle ride quality estimation. As suggested by an anonymous

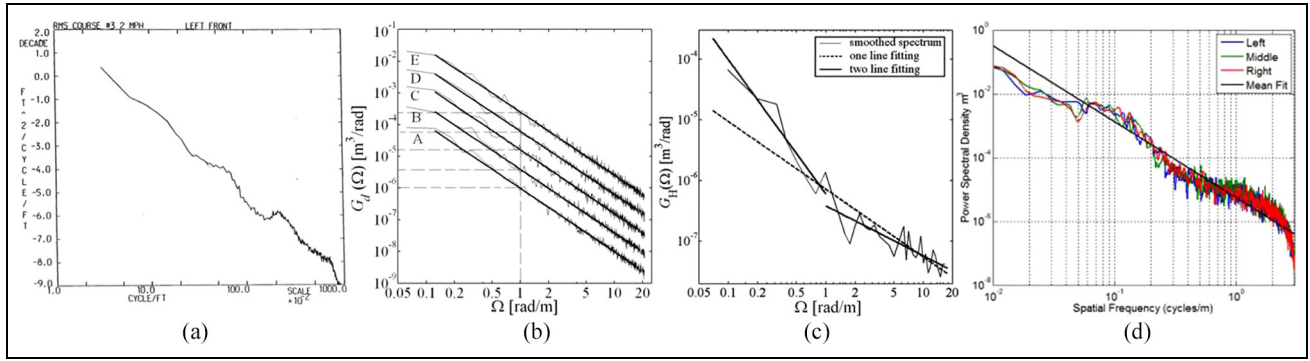


**Figure 7.** (a) Yuma proving ground rough road course,<sup>26</sup> (b) simulated road profiles characterized by unevenness index  $C$  or  $G_d(\Omega_0) = 1, 4, 16, 64,$  and  $256e-6 \text{ m}^3/\text{rad}$ ,<sup>27</sup> (c) Portland cement concrete (PCC) road profile with potholes measured in Indiana (road section LTPP 18060211),<sup>28</sup> and (d) rough asphalt road at the National Center for Asphalt Technology (NCAT) test track in Opelika, Alabama.<sup>29</sup>

**Table 5.** Longitudinal spacing (brick size) and highest and lowest point difference (Max-Min) of different pave tracks.

Track	Brick size (mm)	Max-Min (mm)
NATRiP	150	220
Gerotek	130	180
Daimler AG	165	140

reviewer, we have compared the PSDs of our pave track with two other well-known pave tracks (Gerotek<sup>23</sup> and Daimler AG Stuttgart-Unterturkheim).<sup>30</sup> The paving details of these tracks are shown in Table 5 and the PSDs are shown in Figure 8. The displacement profiles of the Daimler AG track are readily available from OpenCRG@.<sup>31</sup> These profiles were used to perform additional new vehicle simulation results which are discussed in section “Results.”

We now present our detailed simulation results along with experimental measurements.

## Results

The vertical acceleration measurements were recorded at 100 Hz. For subsequent comparisons with ADAMS, the test data was low pass filtered with a cut-off frequency of 30 Hz using MATLAB’s `designfilt`.

In ADAMS simulations, displacement inputs were applied at each wheel contact point  $C_i$ . The vertical acceleration responses at wheel axle points  $A_i$  and body points  $B_i$  were computed and subsequently compared against the test data. For deterministic simulations (continuous displacement case), for a given test, the same interval of time was used to compare all

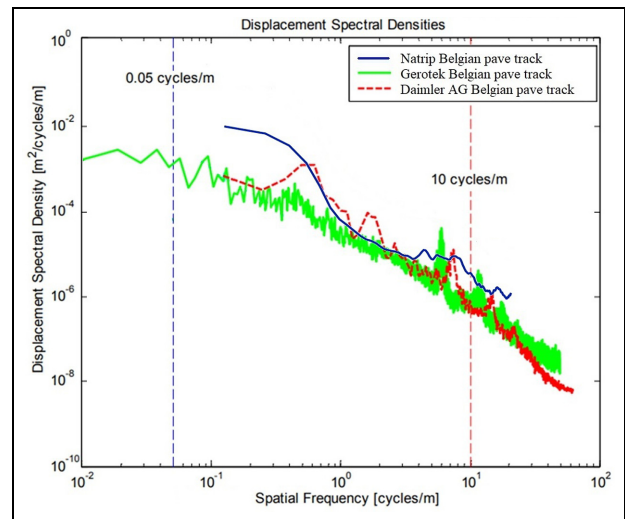


**Figure 8.** Elevation PSDs of different pave tracks. Source: Adapted from Becker and Els.<sup>23</sup>

accelerometer outputs. For stochastic inputs (Belgian pave), ADAMS does a frequency domain calculation directly.

We now represent a detailed discussion of the simulation and test results for the low-severity washboard track. For all other tests, a representative subset of results is given for the sake of brevity. Detailed results are available in the literature.<sup>22</sup>

### Low-severity tracks

**Washboard track.** A discussion of the test response of the front left wheel axle  $A_1$  and the corresponding response of the suspension-to-body attachment point  $B_1$ , for a

low-severity washboard track, is now given as a typical example of test results.

For ADAMS simulation, the wheel displacement input is obtained from the rigid-road contact model and is applied at wheel contact point  $C_1$ ; see the plot in Figure 9(a). Corresponding to the wheel input there is an axle response and a body point response, as shown in Figure 9(b). The axle response at  $A_1$  (ADAMS model and field test) is shown in Figure 9(c).

We observe that the widths of the periodic responses are correct on the whole, and the peaks are comparable; the rapid oscillations near the bottom are not fully captured, most likely due to unmodeled flexibility effects in the frame and/or driver. The forward speed of the vehicle shows some variation that is not captured in the present approach. Finally, we have observed from simulations with other parameter values that the wheel compliance and damping significantly affect the axle response; and the match obtained deteriorates if we change the wheel stiffness and damping parameters significantly. To this extent, we conclude that the wheel stiffness and damping parameters in the model are accurate.

The body point response at  $B_1$  is similarly shown in Figure 9(d). Here too, the peak heights and the widths are roughly matched by the simulation. Overall, the ADAMS model reasonably correlates with the field test measurements. We conclude that the inertial and compliance properties of the overall vehicle model are fairly accurate.

For both axle and body point responses, there is apparently a low-frequency fluctuation in amplitude and phase. This could be due to a slight asymmetry in suspension parameters, a somewhat weak excitation of a roll mode, or even an approximately periodic fluctuation in the forward speed of the vehicle during testing. We are not able to resolve this issue because the vehicle was manually driven.

There is also a relatively higher frequency component in the field data ( $\sim 10$  Hz), which we believe is from the engine and transmission of the ATV, and therefore missing from the ADAMS simulation results. This will be more visible in the chassis twist track results below.

Other simulation results, obtained with the same model parameters and given in Figure 10, show that the quality of the match with the field test responses remains about the same. The accelerations of body points  $B_1$  through  $B_4$  are denoted by  $\ddot{x}_1(t)$  through  $\ddot{x}_4(t)$ , and the accelerations of wheel axle points  $A_1$  through  $A_4$  are denoted by  $\ddot{y}_1(t)$  through  $\ddot{y}_4(t)$ . The thicker lines show test data.

Having presented the washboard track results in some detail, for subsequent tests on other tracks we will present results only for points at the front left location (axle point  $A_1$  and body point  $B_1$ ). Further details, as mentioned above, are available in the literature.<sup>22</sup>

**Herringbone track.** Figure 11 shows a representative sample of simulation and test results for the low-severity herringbone track. The peak heights and the peak widths match well on the whole.

**Chassis twist track.** On this 4-m-wide track, the vehicle was driven on the left side of the track, and the corresponding road inputs given to the ADAMS model. Figure 12 compares simulation and test results for the low-severity chassis twist track. The peak heights and widths match, but there is a high-frequency component ( $\sim 10$  Hz) in the field data, which we believe is from the ATV engine and transmission (engine:  $\sim 1800$  r/min, CVT: reduction ratio  $\sim 3$ , hence 600 r/min or 10 Hz).

We now present results for high-severity tracks.

### High-severity tracks

**Washboard track.** Figure 13 shows the comparison of simulation and test results of high-severity washboard track. The peak heights and widths match reasonably well for the axle point  $A_1$ . The high-frequency component from the engine and transmission now has a higher frequency because of the higher engine speed and lower reduction ratio of the CVT. The peaks of the response at body point  $B_1$  are narrower than that in simulation, indicating different harmonic content at the same fundamental frequency. One possible reason for the mismatch being pronounced in this more severe test case is that forward speed fluctuations are higher. Such fluctuations in forward speed could, for example, set up pitching oscillations that the simplified ADAMS model cannot capture under purely vertical base excitation.

**Herringbone track.** Figure 14 compares simulation and test results for the high-severity herringbone track. Since the bumps do not hit the right and left wheels simultaneously, the right- and left-side responses of the vehicle are not in phase. However, we show the front left responses only, as mentioned above. There is now an observable systematic mismatch between simulation and test results. The axle responses in the field data are smaller: we believe this is because of wheel compliance effects, which are neglected in our kinematic ground-



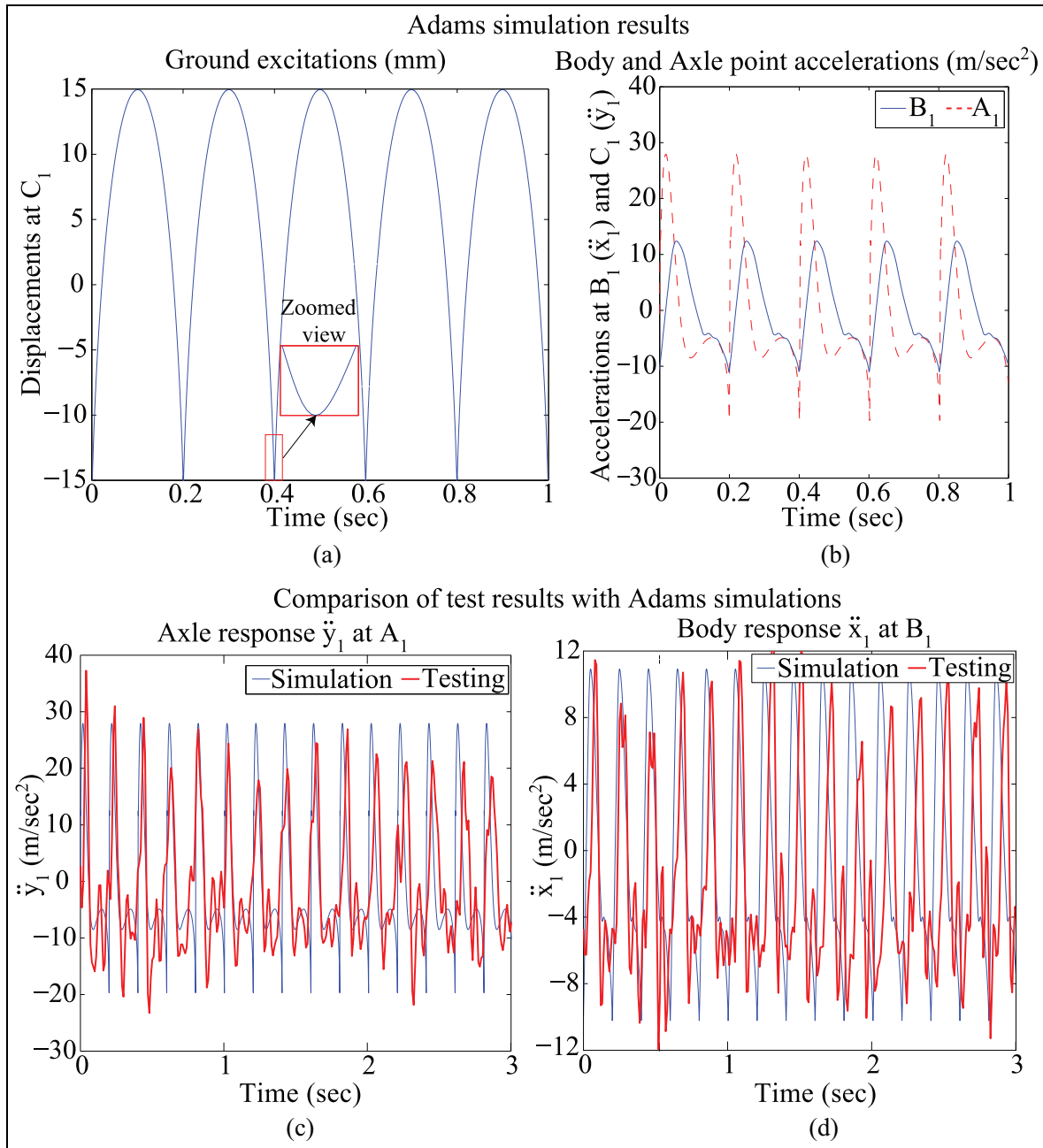


**Figure 9.** (a) Ground displacement input at  $C_1$  given to the ADAMS model (see ② in Figure 2), (b) axle and body point responses obtained from ADAMS simulation, (c) response  $\ddot{y}_1(t)$  of front left axle  $A_1$ , and (d) response  $\ddot{x}_1(t)$  of suspension to body attachment point  $B_1$ . The thicker line shows test data.

wheel contact model. Simultaneously, the body point accelerations are *not* smaller in the field data. The excitation to the body passes through the axle, which means that the simulated body point response is, relatively

speaking, smaller. We believe this relative increase in the body response for field data is due to the stiffening nonlinearity of the suspension (recall Figure 1(b)), which is not incorporated in the ADAMS model.

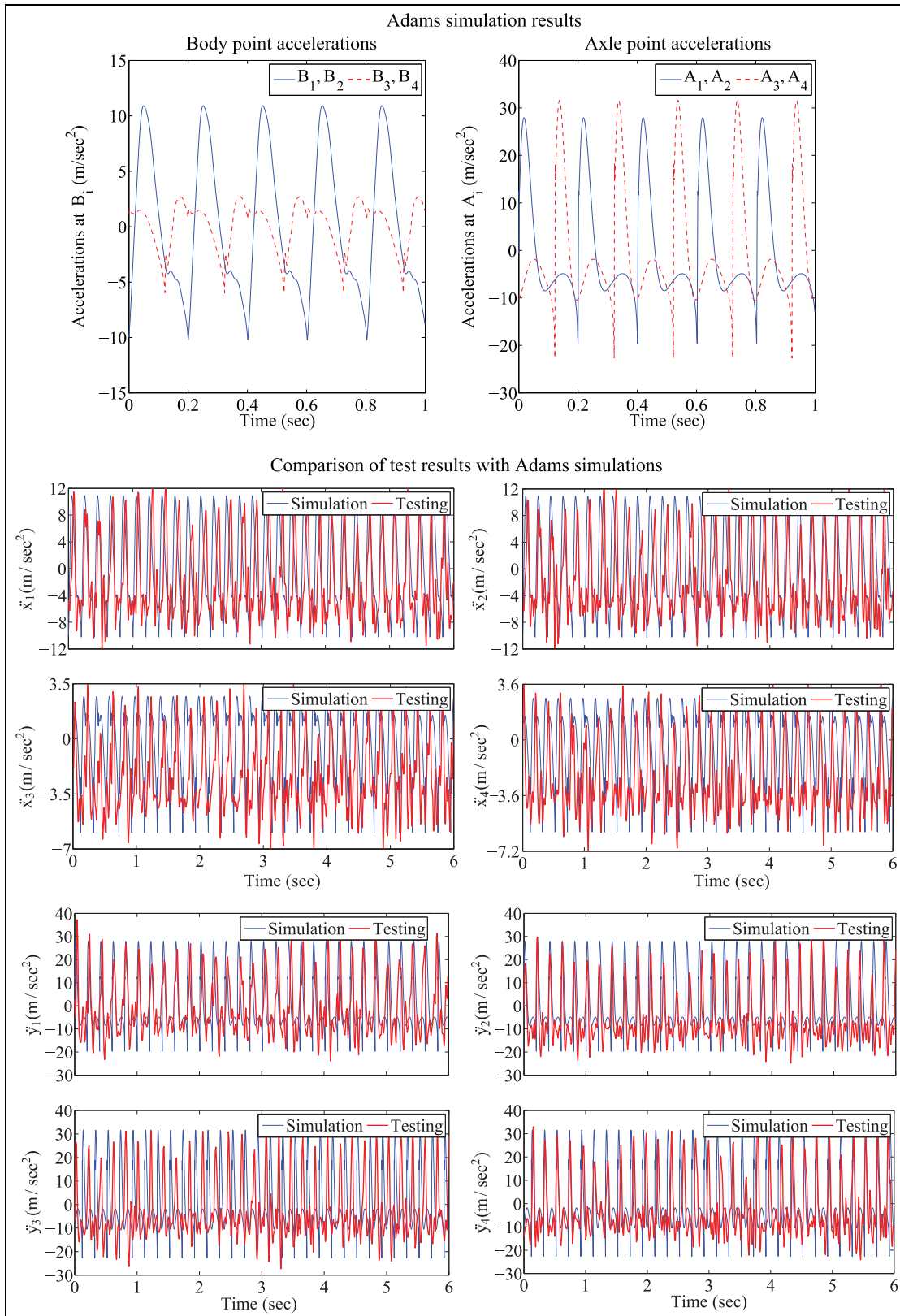
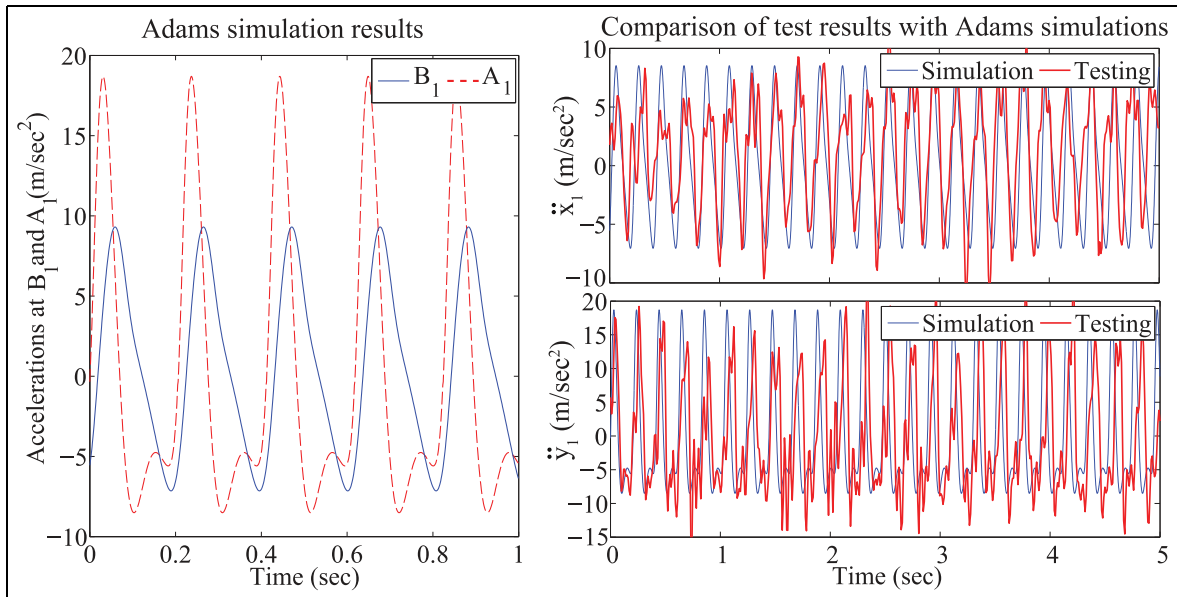
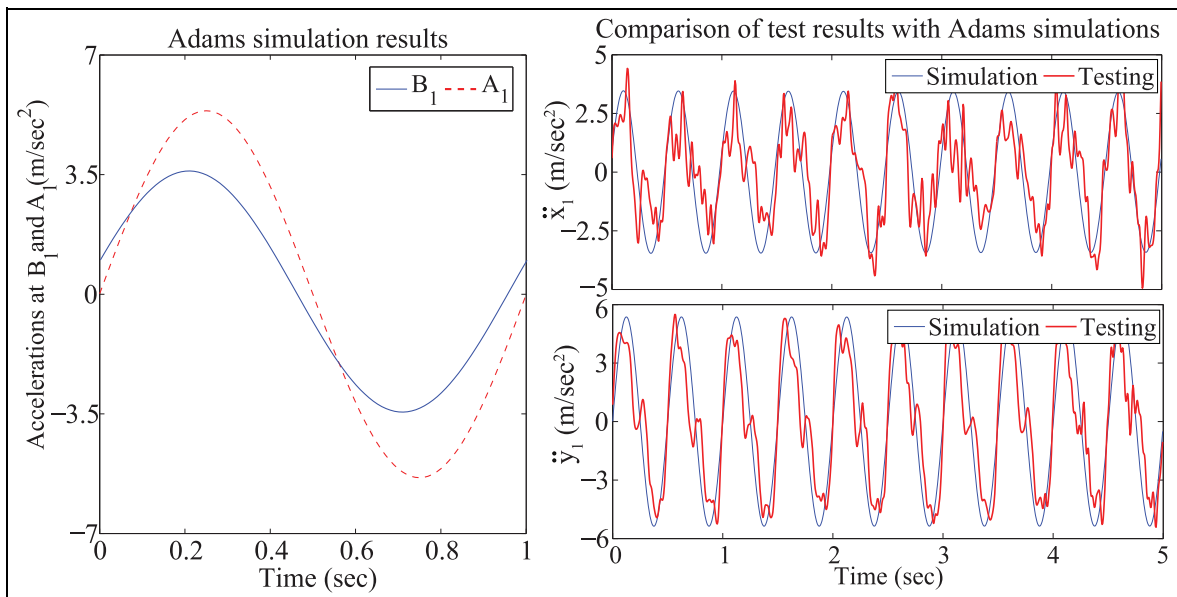


Figure 10. Results for the low-severity washboard track.



**Figure 11.** Results for the low-severity herringbone track.



**Figure 12.** Results for the low-severity chassis twist track.

*Chassis twist track.* Figure 15 shows results for the high-severity twist track. The peak heights and the peak widths roughly match, but the slowly increasing divergence between simulation and test data is visible. Tire compliance and suspension nonlinearity play a significant role in this test. The high-frequency component from the engine and transmission is clearly visible as well.

*One-sided washboard track.* We now come to our final test with deterministic track inputs. Figure 16 shows results for the high-severity one-sided washboard track. In this case, there is a relatively large mismatch between ADAMS simulation test track measurements. In this test, the vehicle undergoes significant rocking motions. Due to the rocking motions, the driver should not be modeled as rigid. Moreover, the driver uses his arms

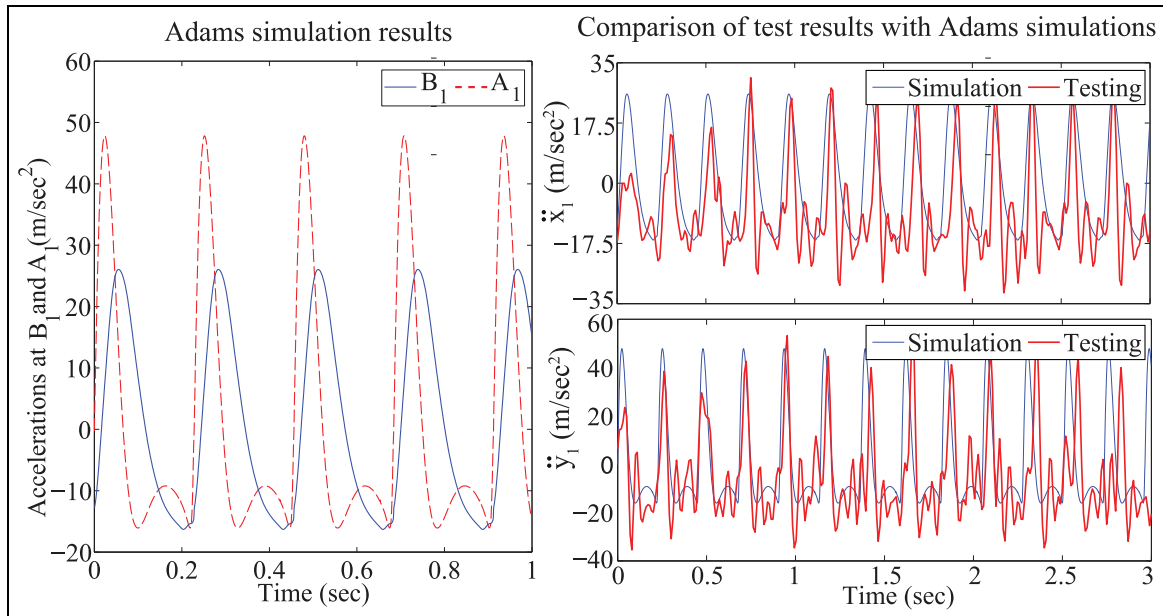


**Figure 13.** Results for the high-severity washboard track.

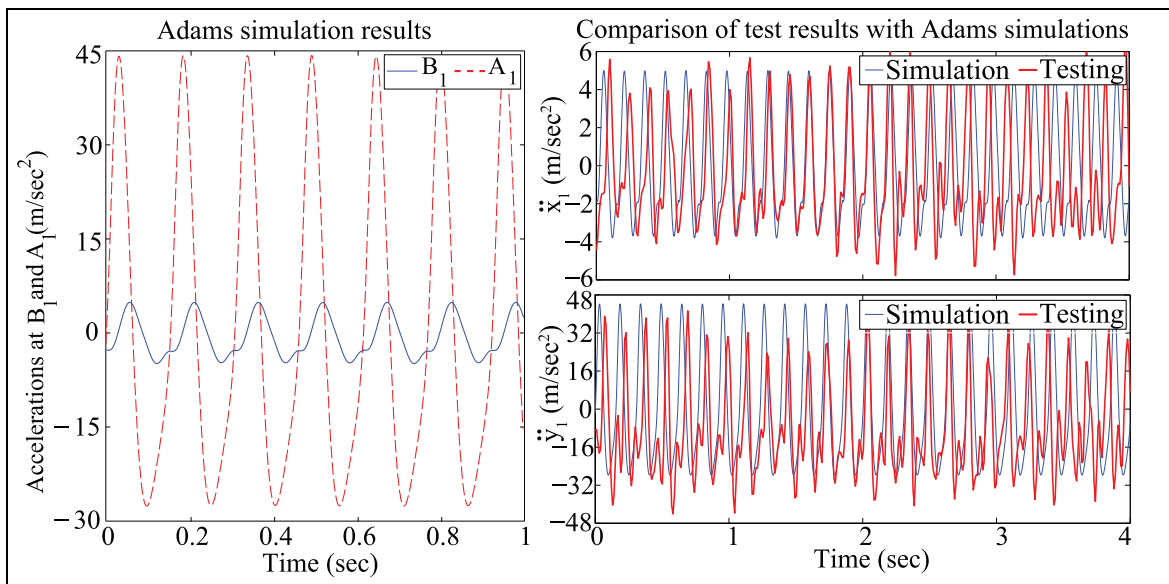


**Figure 14.** Results for the high-severity herringbone track.

and muscles to resist motion relative to the vehicle, and so there is a coupling between the driver and the vehicle which is not easy to model, and certainly not captured in the ADAMS model.

Future work may take up such modeling.

So far we have seen that the model simulation results match well with experimental data for tests performed on different deterministic tracks. In order to provide a quantitative measure of model fitting, we

have used normalized root mean square deviation (NRMSD) to compare the front left body and axle point responses against the test data. Normalizing the root mean square deviation (RMSD) facilitates the comparison between data sets or models with different scales. We have used the range (the maximum value minus the minimum value) of the measured test data for normalization.

NRMSD is defined as

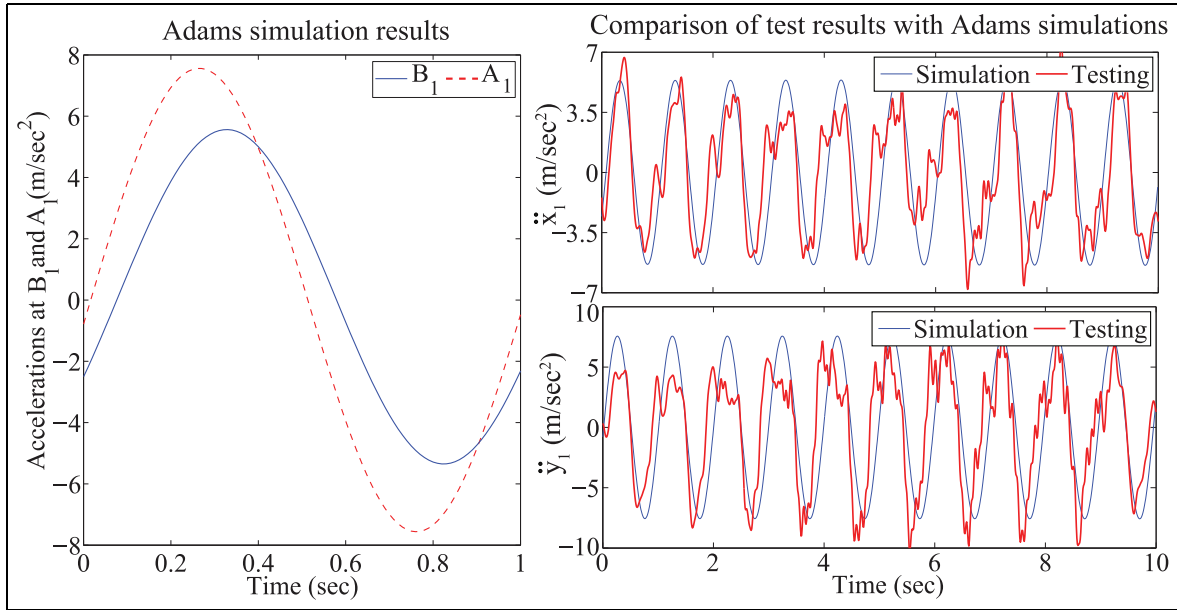


**Figure 15.** Results for the high-severity chassis twist track.

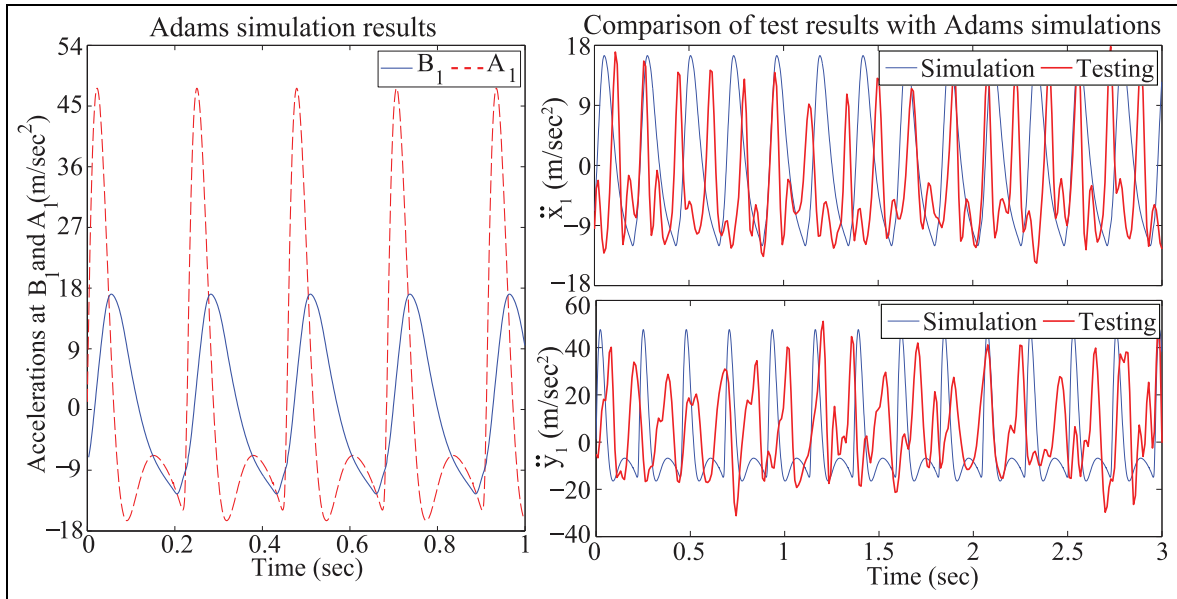


**Figure 16.** Results for the high-severity one-sided washboard track.

$$\text{NRMSD} = \frac{\text{RMSD}}{y_{\max} - y_{\min}}; \quad \text{RMSD} = \sqrt{\frac{\sum_{t=1}^T (\hat{y}_t - y_t)^2}{T}} \quad (9)$$

where  $\hat{y}_t$  is the simulated response and  $y_t$  is the test response at time “ $t$ ,”  $y_{\max}/y_{\min}$  are the maximum/minimum values of the test responses, and “ $T$ ” is the total number of samples considered for evaluating the measure of the fit.

The model fitting results in terms of NRMSD are given in Table 6.

Model fitting results suggest that the model matches the experiments well for low speed tests on low-severity tracks (see Table 6). The best fit is obtained for the chassis twist track (0.11) followed by herringbone (0.18) and washboard (0.17) while the correlation for the one-sided washboard track test is poor with a normalized root mean square deviation (NRMSD) of 0.31. This is evident from looking at the model and test comparison plots in Figures 10–16.



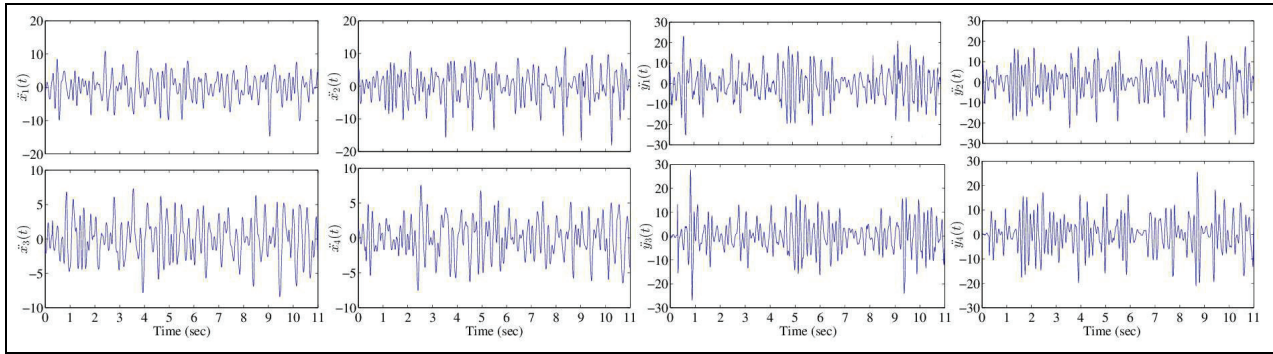


**Figure 17.** Body point accelerations  $\ddot{x}_i$  and wheel axle accelerations  $\ddot{y}_j$  for vehicle testing on pave track.

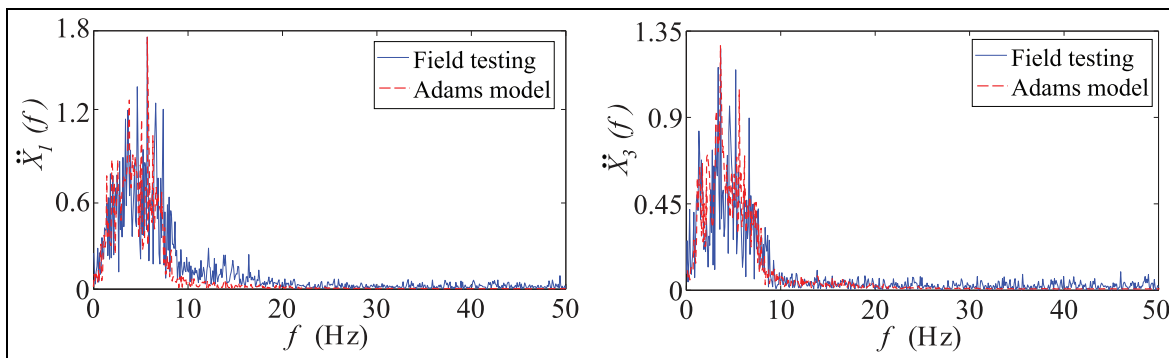


**Figure 18.** Comparison of acceleration FFT magnitudes at body points  $B_1$  and  $B_3$ .

**Table 6.** Model fitting results (NRMSD) for body point  $B_1$  and axle point  $A_1$ .

Track	Severity	$B_1$	$A_1$
Washboard	Low	0.27	0.17
	High	0.24	0.22
Herringbone	Low	0.17	0.18
	High	0.23	0.25
Chassis twist	Low	0.11	0.14
	High	0.15	0.16
One-sided washboard	Low	0.31	0.25

NRMSD: normalized root mean square deviation.

### Belgian pave track

We finally consider the Belgian pave track, which is modeled in the frequency domain as mentioned earlier. The test driving speed was 12 kmph. Time series acceleration measurements from the vehicle are shown in Figure 17 for all four axle and wheel locations. It is noted that forward body point accelerations  $\ddot{x}_1$  and  $\ddot{x}_2$  are significantly larger, on average, than the rearward body point accelerations  $\ddot{x}_3$  and  $\ddot{x}_4$ , because the weight in the vehicle is toward the rear. For axle point accelerations  $\ddot{y}_1$  through  $\ddot{y}_4$ , the magnitudes are comparable

because all wheels experience similar forcing from the cobbled track.

Finally, ADAMS simulation results for front left and rear left body points  $B_1$  and  $B_3$  are compared with test results in the frequency domain in Figure 18. The ADAMS model matches the test data well for frequencies up to 10 Hz. Note that some individual peaks are missed because the excitation used in the simulations has no frequency peaks in it and is a simple power law fit, while stretches of test data may have almost-periodic windows yielding such peaks in a non-repeatable way.

### Comparison against other standard tracks: Daimler AG Belgian pave

As discussed earlier, our methodology can be used for suspension model validation using a wide variety of test tracks. In this section, we demonstrate the model simulation results for the Daimler AG Belgian pave test track. Both front and rear track widths of our vehicle is 1.2 m. The ground elevations of the left ( $Y = -0.6$  m) and right ( $Y = 0.6$  m) tracks are obtained from the test track data available at OpenCRG® (see Figure 19). The vehicle speed of 12 kmph is chosen for the

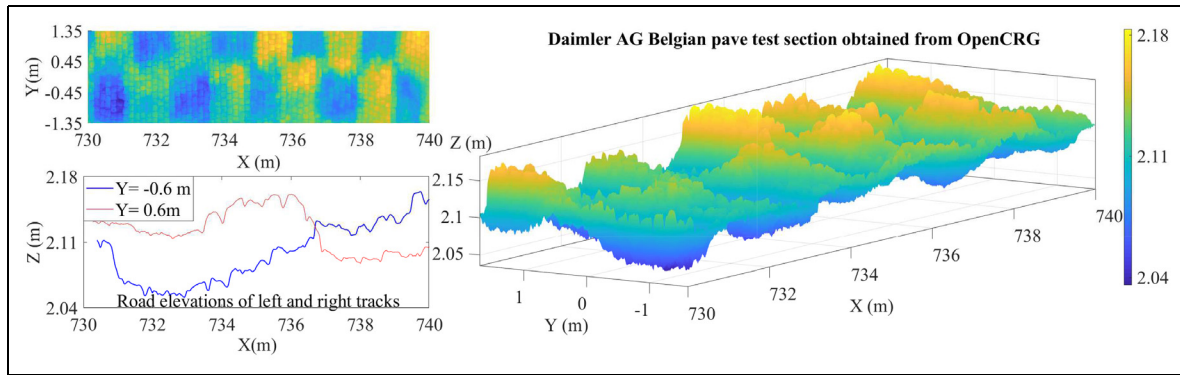


**Figure 19.** Ground elevations at left and right tracks obtained from the PSD of the Daimler AG Belgian pave track data.<sup>30,31</sup>

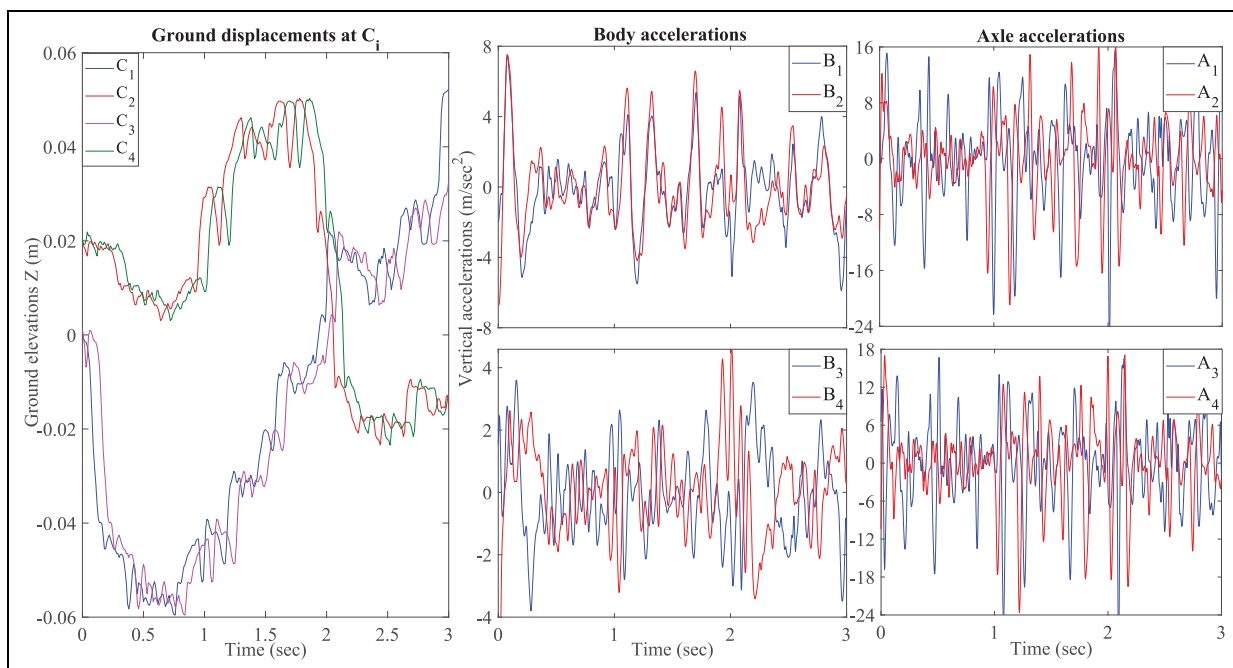


**Figure 20.** Vehicle simulation results on Daimler AG Belgian pave track.

simulation. (The vehicle speed for this simulation is the same as that of the Belgian pave track test at NATRiP in order to compare the relative magnitudes of the body and axle point accelerations.) These ground displacements are assigned to the wheel contact points  $C_1$  through  $C_4$  and the acceleration responses at the axle point  $A_i$  and the body point  $B_i$  are obtained from the ADAMS model (see Figure 20).

It can be seen that the magnitudes of the axle and body point accelerations are comparatively lower for this track as compared to the Belgian pave track of NATRiP. This is because of the reason that the latter track is more severe as it is designed more from vehicle durability point of view than ride. However, the statistical fluctuations of the responses for both the tracks match and the peak widths and transients are roughly the same.

### *Effect of frame flexibility*

In this study, we have used the FE model of the chassis to capture the effects of frame flexibility. The vehicle chassis flexes substantially while running on high-severity accelerated durability tracks (ADT). The suspension links are rigid enough so the flexibility of the linkages was neglected. Moreover, the complexities of suspension linkage kinematics were overcome using a motion ratio to obtain the effective stiffness and damping properties at the wheels.

Frame flexibility strongly affects the vertical acceleration responses of the vehicle body and it is critical to account for flexibility of the frame in modeling the vehicle suspension system.<sup>32</sup> As suggested by an anonymous reviewer, we have compared the body point responses of the flexible FE chassis model with that of the rigid

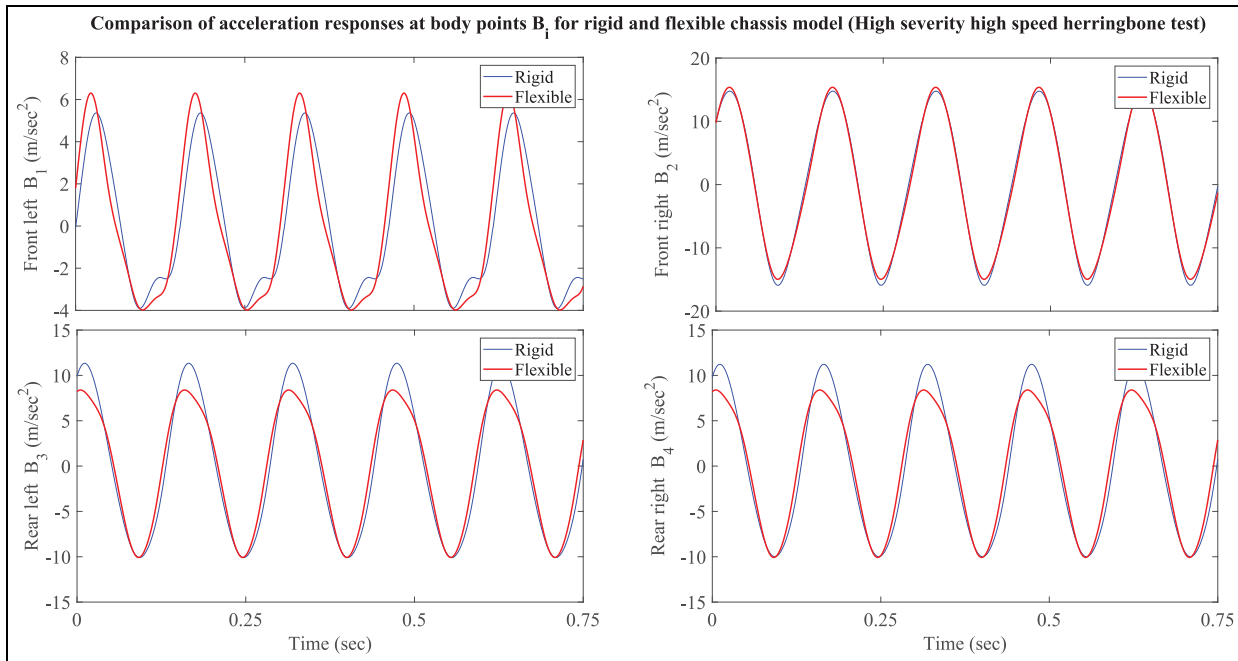


**Figure 21.** Comparison of the simulation results of the acceleration responses  $\ddot{x}_i$  of all body points  $B_i$  for rigid and flexible chassis model.



**Figure 22.** Some places where the tracks are not straight.

chassis model. The scenario considered for the comparison is the high-speed high-severity herringbone track test. The results are shown in Figure 21.

It is evident from Figure 21 that the flexibility of the frame cannot be neglected. Although frame flexibility can be switched off to obtain a more simplified version of the model (rigid chassis) for simulating low-speed vehicle response on low-severity test tracks. (This is because at low speeds and on low-severity tracks the frames flexes by only a small amount and the response obtained from the rigid and flexible chassis model is nearly identical.)

## Discussion and conclusion

Partial validation of a simplified ADAMS model for an ATV has been conducted using field test results.

Such simplified modeling captures essential vertical dynamic characteristics of the vehicle suspension. The present approach of using test track data for model validation seems useful when the vehicle in question is small, the rider is relatively heavy, the track is uneven, and actual vehicle behavior under human rider control is of interest.

The simulation results match experiments reasonably well for low-severity tracks. The mismatch is greater for high-severity tests, essentially because of dynamic issues not incorporated in the simple ADAMS model. Some possible reasons for such mismatch are discussed below.

The displacement inputs used in simulation are smoother than actual wheel displacement inputs because of unmodeled small-scale roughness of the road surface. A high-frequency vibration due to engine

and transmission exists in the actual vehicle but not in the ADAMS model. When the vehicle moves on a severely undulating track, the human driver cannot maintain a constant speed and the resulting longitudinal accelerations cause pitching oscillations, not included in the present level of ADAMS modeling, which has purely vertical base excitations. The vehicle does not have a differential, so wheel slip may occur; but such slip has not been modeled. Dynamic consequences of the shifting location of actual ground-wheel contact have not been modeled. The test tracks are curved at some places, but such lateral dynamics have not been modeled (see Figure 22). On the one-sided washboard tracks, the vehicle undergoes rocking motions wherein a coupling between the driver and the vehicle may come into play, but such dynamics have not been modeled. Finally, in the real vehicle, there are other unmodeled effects like backlash, loose joints, and suspension nonlinearity, which have not been modeled.

Nevertheless, the overall match is good, in the sense that the peak magnitudes of accelerations on the axle and body points have been fairly well captured, and the widths of the non-sinusoidal peaks have been reasonably captured in most cases as well. These two aspects suggest that on the whole, from a suspension dynamics viewpoint, the ADAMS model captures the effects of vehicle mass distribution, other-wheel effects at each suspension spring location, frame flexibility, and damping. The approach proposed in this article is generic and can be used for a wide variety of test tracks. We have simulated our model on openly available test track model of Daimler AG pave track from OpenCRG®. Finally, in order to demonstrate the effect of frame flexibility, a model comparison study was done where the body point acceleration responses of the rigid chassis model is compared with that of the flexible chassis model. We have found that chassis flexibility plays an important role in determining the vibration response of the vehicle body.

The complete exercise also serves to provide useful understanding of issues that cause differences between simplified vertical-excitation dynamics in the ADAMS model and the fully three-dimensional human-driven prototype vehicle.

### Acknowledgements

We thank N. Karuppaiah, Additional Director, NATRiP, Indore for use of the facilities there; Vinod Pare of SGSITS, Indore for use of the Baja ATV for field test; Amit Singh, Jay Pratap, and Suraj Mishra of SGSITS, Indore and Vaibhav Dhar Dwivedi of IIT Kanpur for help with the experiments; and Sagar Bendre of NATRiP for sharing general expertise on several important areas.


### Declaration of conflicting interests

The author(s) declared no potential conflicts of interest with respect to the research, authorship, and/or publication of this article.

### Funding

The author(s) disclosed receipt of the following financial support for the research, authorship, and/or publication of this article: The authors acknowledge the financial support provided by Innovate UK under the project grant MuCCA “Multi-Car Collision Avoidance,” comprised by the consortium with Applus-IDIADA, Cosworth Electronics, Transport Systems Catapult, Westfield Sportscars, and Cranfield University.

### ORCID iD

Husain Kanchwala  <https://orcid.org/0000-0002-1369-3833>

### References

1. MD-ADAMS, <http://web.mscsoftware.com/Products/CAE-Tools/MD-Adams.aspx> (accessed 10 November 2015).
2. Ning X, Zhao C and Shen J. Dynamic analysis of car suspension using ADAMS/Car for development of a software interface for optimization. *Procedia Engineer* 2011; 16: 333–341.
3. Azadi S, Vaziri M and Hoseini M. Vehicle dynamic control of a passenger car applying flexible body model. *Vehicle Syst Dynam* 2010; 48: 587–617.
4. Chindamo D, Gadola M and Marchesin F. Reproduction of real-world road profiles on a four-poster rig for indoor vehicle chassis and suspension durability testing. *Adv Mech Eng* 2017; 9: 1–10.
5. Braghin F, Cheli F, Genoese A, et al. Experimental modal analysis and numerical modelling of agricultural vehicles. In: *Proceedings of the IMAC-XXVII*, Orlando, FL, 9–12 February 2009. Bethel, CT: Society for Experimental Mechanics Inc.
6. Melzi S, Negrini S and Sabbioni E. Numerical analysis of the effect of tire characteristics, soil response and suspensions tuning on the comfort of an agricultural vehicle. *J Terramechanics* 2014; 55: 17–27.
7. Banerjee S, Balamurugan V and Krishnakumar R. Ride dynamics mathematical model for a single station representation of tracked vehicle. *J Terramechanics* 2014; 53: 47–58.
8. Els P, Theron N, Uys P, et al. The ride comfort vs. handling compromise for off-road vehicles. *J Terramechanics* 2007; 44: 303–317.
9. Mini-Baja SAE India, <http://www.bajasaehindia.org/> (accessed 3 March 2017).
10. Mishra S and Goyal V. Vehicle #007. Team GS racers design report, 2016, <https://perma.cc/Y334-VLUM>
11. Els P. The applicability of ride comfort standards to off-road vehicles. *J Terramechanics* 2005; 42: 47–64.

12. MTS 85025. Model 850 load unit product manual, <https://tinyurl.com/y6pstvtl> (accessed 3 March 2017).
13. FOX Float 3/Float 3 EVOL R. Factory series owners manual, [http://www.ridefox.com/fox\\_tech\\_center/owners\\_manuals/605-00-119-revA.pdf](http://www.ridefox.com/fox_tech_center/owners_manuals/605-00-119-revA.pdf) (accessed 3 March 2017).
14. Kanchwala H and Chatterjee A. A generalized quarter car modelling approach with frame flexibility and other nonlocal effects. *Sādhanā* 2017; 42: 1175–1192.
15. Rollcage. Material testing report, 2015, <https://tinyurl.com/hp821>
16. Hanavan EP Jr. A mathematical model of the human body. Technical Report, Defense Technical Information Center, Fort Belvoir, VA, October 1964.
17. Chandler R, Clauser C, McConville J, et al. Investigation of inertial properties of the human body. Technical Report, Defense Technical Information Center, Fort Belvoir, VA, March 1975.
18. BKT ATV Tyres, <https://www.bkt-tires.com/en/pattern/w-207> (accessed 3 March 2017).
19. Wong J. *Theory of ground vehicles*. New York: John Wiley & Sons, 2008.
20. NATRAX, <http://www.natrip.in/index.php/natrax-about-testing-centers> (accessed 10 November 2016).
21. Saxena A and Sahay B. *Computer aided engineering design*. Berlin: Springer Science & Business Media, 2007.
22. Kanchwala H. *Studies in simplified dynamic modeling and characterization of vehicle suspensions*. PhD Thesis, Indian Institute of Technology, Kanpur, India, 2017, <https://perma.cc/QQ5Q-C9JW>
23. Becker C and Els P. Profiling of rough terrain. *Int J Vehicle Des* 2014; 64: 240–261.
24. González A, O'Brien E, Li Y, et al. The use of vehicle acceleration measurements to estimate road roughness. *Vehicle Syst Dynam* 2008; 46: 483–499.
25. ISO 8608:2016. Mechanical vibration—road surface profiles—reporting of measured data, 2016.
26. Ashmore S, Hodges H Jr and Prebeg M. Terrain severity data generation at Yuma Proving Ground, vol. 2. *Technical report, Nevada Automotive Test Center, Carson City, NV*, November 1990.
27. Múčka P. Simulated road profiles according to ISO 8608 in vibration analysis. *J Test Eval* 2017; 46: 1–14.
28. Múčka P. Longitudinal road profile spectrum approximation by split straight lines. *J Transp Eng* 2011; 138: 243–251.
29. Dawkins J. *Terrain characterization and roughness estimation for simulation and control of unmanned ground vehicles*. PhD Thesis, Auburn University, Auburn, AL, December, 2011.
30. Belgian block road sample of Daimler durability test track, <http://maps.google.com/maps?&q=48.7860,9.2331> (accessed 3 March 2017).
31. OpenCRG<sup>®</sup>, <http://www.opencrg.org/> (accessed 15 February 2016).
32. Ibrahim I, Crolla D and Barton D. Effect of frame flexibility on the ride vibration of trucks. *Comput Struct* 1996; 58: 709–713.